**Received:** 01 July 2026; **Revised:** 20 August 2026; **Accepted:** 12 September 2026; **Published:** 18 October 2026
*Archs Sci. (2026) Volume 76(4), Pages 212-224, Paper ID 2026423.*
*https://doi.org/10.68304/as/76423*

# Voltage Quality Control Method for a Distribution Station Area Based on an Improved Particle Swarm Optimization Algorithm

**Jian Liu[1], Hui Fu[1], Mingming Shi[1], and Xian Zheng[2]**
[1]State Grid Jiangsu Electric Power Research Institute Co., Nanjing 210000, Jiangsu, China
[2]State Grid Jiangsu Electric Power Co., Nanjing 210000, Jiangsu, China
Corresponding author: Jian Liu (e-mail: liuj@js.sgcc.com.cn).

**Abstract** The integration of distributed photovoltaic (PV) generation into distribution networks can degrade voltage quality by changing feeder power flows, increasing voltage deviations, and aggravating three-phase voltage unbalance. To address these operational challenges, this study develops a coordinated voltage quality regulation method for a low-voltage distribution station area using an improved particle swarm optimization (PSO) algorithm. Effective voltage regulation is increasingly important for maintaining reliable and efficient distribution network operation as the penetration of variable renewable generation continues to grow. The proposed approach first examines the effects of individual and multiple PV connections on nodal voltages and phase unbalance. It then evaluates the regulation mechanisms of reactive power compensation devices, including capacitor banks and the available reactive power resources of distributed PV systems. By modifying the inertia weight, dynamically adjusting learning factors, and incorporating a neighborhood reference into the PSO search process, the method seeks an improved solution to a multi-objective voltage regulation problem. A 380-V low-voltage distribution network in Jiangsu Province, China, is used to assess the proposed coordination strategy through simulation. Relative to independent reactive power regulation, the coordinated approach reduces the reported main-feeder voltage deviation by an average of 30.72% during the daytime evaluation period and improves the three-phase voltage unbalance at representative nodes. These results indicate that the coordinated use of existing compensation equipment and distributed PV reactive power can improve voltage profiles and phase balance without introducing additional compensation devices in the simulated system. The proposed multi-objective method therefore provides an applicable framework for jointly considering voltage deviation, unbalance, operating constraints, and control-resource coordination in PV-rich station areas.

**Index Terms** Voltage quality, distributed photovoltaic (PV) generation, particle swarm optimization (PSO), reactive power compensation, voltage regulation, three-phase voltage unbalance.

## I. Introduction

The mechanisms responsible for the formation and propagation of voltage quality disturbances in active distribution networks become increasingly complex as distributed photovoltaic (PV) generation is integrated at high penetration levels [1]–[3]. Conventional monitoring and control methods, which are frequently designed for a single load, a single distributed source, or one voltage quality indicator, may not adequately address the interactions between generation, loads, feeder impedance, and unbalanced phase connections [4]–[6]. These limitations complicate reliable network operation and can prevent distribution operators from realizing the full operational benefits of distributed generation [7], [8]. Consequently, station-area voltage regulation requires a coordinated strategy that addresses voltage deviation, phase unbalance, and the technical limits of controllable reactive power resources simultaneously.

Previous investigations have described the influence of distributed PV and other distributed energy resources on network power flows, voltage profiles, power quality disturbances, and additional electrical losses [9], [10]. A review of power quality disturbance monitoring and mitigation methods identified the roles of compensation devices, harmonic filters, and coordinated control in distribution systems [11]. Research on power-electronic controllers has also examined harmonic reduction and current quality enhancement through converter modulation and optimization techniques [12], while adaptive multi-second-order generalized integrator-based reference current generation has been investigated for PV-connected converter control [13]. These studies establish the importance of flexible compensation, although not all directly optimize the combined voltage deviation and three-phase unbalance of a low-voltage station area.

The development of multifunctional grid-connected converters offers additional means of providing reactive power support and harmonic compensation alongside renewable

electricity generation [14]. Station-area research has specifically addressed overvoltage, harmonics, and reverse power flow associated with the increasing deployment of distributed PV in low-voltage rural networks [15]. Other research has demonstrated that coordinating PV reactive power with conventional voltage control equipment can improve nodal voltage regulation and distribute the compensation burden among PV resources [16]. System-level assessment frameworks have also been formulated to evaluate the voltage quality of radial distribution networks with distributed generation [17]. Investigations of large-scale PV integration further emphasize the operational challenges of maintaining voltage quality and managing reactive power across multiple network locations [18]. An analytic hierarchy process (AHP)-based evaluation framework has been developed to aggregate several voltage quality indices into an overall assessment indicator [19].

Beyond voltage quality evaluation, recent work has examined phase-unbalance mitigation through coordinated adjustable resources [20] and integrated voltage regulation strategies for distribution station areas [21]. Related studies have employed improved particle swarm optimization (PSO) for coordinated loss reduction and dispatch in active distribution systems [22]. Site-selection models combining fuzzy hierarchical analysis and PSO demonstrate the wider applicability of swarm-based optimization in PV planning [23], while PSO-based learning models illustrate its usefulness for parameter selection in other electricity-system applications, including charging-load prediction [24]. These related approaches offer useful optimization concepts; however, their objectives differ from the simultaneous regulation of station-area voltage deviation and three-phase unbalance examined here. A control strategy must therefore account for the location-dependent voltage response to PV injection, phase-specific compensation needs, and the discrete or continuous operating limits of available reactive power equipment.

To address the deterioration of voltage quality caused by distributed PV connections while limiting additional compensation costs, this paper proposes a station-area voltage regulation method based on an improved PSO algorithm. The method analyzes the sensitivity of nodal voltage to PV active and reactive power, examines the regulating action of existing compensation devices, and incorporates voltage deviation and three-phase unbalance into a weighted objective function. Its emphasis is on coordinating available station-area resources rather than installing a separate control device for each voltage quality problem. The proposed algorithm combines adaptive inertia weights, dynamically adjusted learning factors, and information obtained from neighboring particles to support a more flexible optimization search. The main contributions are summarized as follows:

1) The effects of both single-PV and multi-PV integration on nodal voltage profiles and three-phase voltage unbalance in low-voltage station areas are analyzed, with particular attention to feeder location and reactive power variation;
2) The voltage quality regulation capability of particle swarm optimization is enhanced by modifying inertia weights and learning factors and by incorporating a neighborhood-best reference variable into the particle velocity update;
3) The coordinated voltage quality regulation method is evaluated on a representative low-voltage distribution station area in Jiangsu Province, with simulation results used to assess improvements in voltage deviation and phase unbalance.

The remainder of the paper is organized as follows. Section II analyzes the effects of single and multiple PV connections on nodal voltages and three-phase unbalance. Section III describes the voltage regulation mechanisms of reactive power compensation equipment. Section IV presents the improved PSO algorithm and its optimization parameters. Section V formulates the coordinated control objectives and associated operating constraints. Section VI reports and discusses the simulation results, and Section VII summarizes the principal conclusions.

## II. Materials and Methods

### *A. Effects of distributed PV integration on voltage quality*

1) Effects of PV integration on the voltage at grid-connection points

1.1) Single PV connection

Figure 1 shows a simplified low-voltage feeder supplying $n$ users, with one distributed PV unit connected at an intermediate node. Point 0 represents the transformer-side supply node. Because upstream voltage variations induced by changes in station-area current are assumed to be small, the source voltage $U_0$ is treated as constant. Positive power flow is defined in the direction from the upstream network toward the loads, whereas reverse power flow is assigned a negative sign. To simplify the analysis, resistive line losses are omitted from the subsequent approximate derivation. The original study reports that this simplification produces a simulation deviation of no more than 0.4%; this value is retained here as a reported modeling assumption rather than an independently verified accuracy bound. The simplified feeder topology establishes the voltage and power-flow sign conventions.

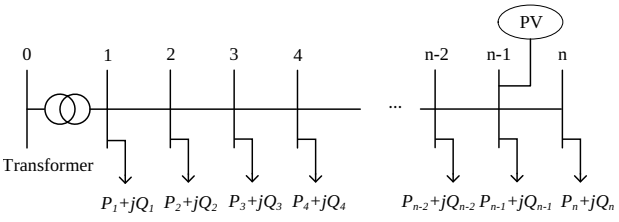


Figure 1: Topology of the low-voltage distribution network with one PV connection

As depicted in Figure 1, the network consists of successive feeder nodes connected by line segments through which active and reactive power are exchanged. The position of the PV connection determines the affected line sections and the

ARCHIVES DES SCIENCES
A Multidisciplinary Journal

locations at which reverse power flow may occur. Accordingly, the discussion below distinguishes between operating conditions dominated by downstream load demand and those in which PV generation exceeds the demand supplied through a particular segment.

When a PV unit is connected to the grid without injecting reactive power, the squared voltage magnitudes at two adjacent points of the feeder are related through the following approximate branch power-flow equation:

$$U_a^2 = U_b^2 - 2(R\,P_{b\to a} + X\,Q_{b\to a}) + (R^2+X^2)\frac{P_{b\to a}^2 + Q_{b\to a}^2}{U_b^2}, \tag{1}$$

where $U_a$ and $U_b$ are the voltage magnitudes at nodes $a$ and $b$, respectively; $P_{b\to a}$ and $Q_{b\to a}$ denote the active and reactive power transferred between these nodes. The parameters $R$ and $X$ represent the resistance and reactance of the relevant line segment, which depend on the corresponding per-unit-length impedance parameters and line length $L$. The symbol $U_{\text{rated}}$ denotes the feeder's rated voltage where a normalized representation is employed.

Eq. (1) describes how branch impedance, active power transfer, and reactive power transfer influence the voltage difference between two adjacent nodes when the PV system supplies no additional reactive compensation. In the particular case where the branch reactive power transfer $Q_{b\to a}$ is zero, the expression reduces to:

$$U_a^2 = U_b^2 - 2R\,P_{b\to a} + (R^2+X^2)\frac{P_{b\to a}^2}{U_b^2}. \tag{2}$$

During ordinary forward-power-flow operation, both the active and reactive powers transferred from node $n-2$ to node $n-1$ are positive under the adopted sign convention. The resulting voltage drop normally makes $U_{n-2}$ greater than $U_{n-1}$. The same principle applies along other feeder segments: positive net power demand generally produces a progressive voltage reduction with distance from the transformer. As local PV generation increases, however, active power may flow backward through the segment. In that case, $P_{n-2,n-1}$ becomes negative while reactive power transfer may remain positive. If the reverse active power is sufficiently large, the voltage at the downstream node can exceed the voltage at the upstream node, so that $U_{n-2} < U_{n-1}$. This explains why voltage rise can become important at PV-rich feeder locations, particularly during periods of high solar generation and relatively low local demand.

Considering the relationships in Eqs. (1) and (2), the effect of a change in branch reactive power on the voltage difference between adjacent nodes can be expressed in the following form. The complex representation also retains the influence of feeder impedance on the voltage phasor.

$$\Delta U_{n-2} = \Delta U_{n-1} + \frac{(x-jr)l_n}{U_N}\Delta Q_{n-2,n-1} \tag{3}$$

Here, $\Delta U_n$ denotes the voltage variation at node $n$, while $\Delta Q_{n-2,n-1}$ denotes the change in reactive power transferred between nodes $n-2$ and $n-1$ following a change in PV reactive power output. The quantities $r$, $x$, and $l_n$ describe the impedance parameters and length of the relevant feeder segment, and $U_N$ is the nominal feeder voltage. This interpretation relates the voltage response to the size of the reactive power adjustment and the electrical distance over which it is transmitted.

When the influence of the quadrature voltage component is neglected in the approximate magnitude calculation, the reactive power dependence of the nodal voltage variation simplifies to the following expression:

$$\Delta U_{n-2} = \Delta U_{n-1} + \frac{xl_n}{U_N}\Delta Q_{n-2,n-1} \tag{4}$$

### 1.2) Multiple PV connections

Figure 2 illustrates a low-voltage distribution feeder serving $n$ users with $m$ distributed PV units connected at different network locations. This representation extends the single-PV analysis to account for the cumulative influence of several generation sources.

The network represented in Figure 2 contains multiple PV connection points distributed along the same low-voltage feeder. Because PV output can vary independently with local operating conditions, the active and reactive power flowing through each branch can change over time. Voltage changes at one connection point therefore depend not only on the local PV output but also on upstream feeder conditions and adjustments made at neighboring PV units. This coupling motivates the use of coordinated rather than isolated reactive power regulation.

Using the same approximate treatment of branch voltage variations, and neglecting the receiving-end quadrature phasor component in the voltage-magnitude calculation, the relationships between the nodal voltage changes and the corresponding changes in branch reactive power can be written as follows. These expressions also include the upper and lower reactive power operating limits of the controllable devices:

$$\begin{cases} \Delta U_1 = \Delta U_2 + \dfrac{xl_n}{U_N}\Delta Q_{12} \\ \Delta U_2 = \Delta U_3 + \dfrac{xl_n}{U_N}\Delta Q_{23} \\ \quad\vdots \\ \Delta U_{n-2} = \Delta U_{n-1} + \dfrac{xl_n}{U_N}\Delta Q_{n-2,n-1} \\ \Delta U_{n-1} = \Delta U_n + \dfrac{xl_n}{U_N}\Delta Q_{n-1,n} \\ Q_{i,\min} \le Q_i \le Q_{i,\max} \end{cases} \tag{5}$$

In Eq. (5), $Q_{i,\min}$ and $Q_{i,\max}$ represent the minimum and maximum reactive power outputs permitted for compensation device $i$, respectively. If the required reactive power for a

ARCHIVES DES SCIENCES
A Multidisciplinary Journal

voltage correction lies outside these bounds, the device output must remain at the appropriate operating limit. Consequently, the available compensation capacity constrains the voltage response that can be achieved throughout the station area.

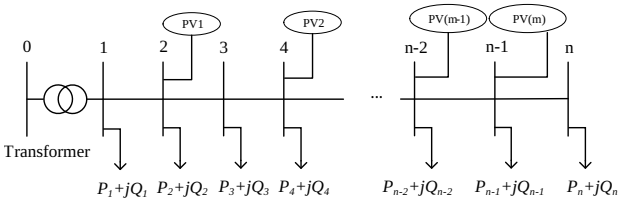


Figure 2: Low-voltage distribution feeder with multiple PV connections

The voltage change at a particular PV node is coupled to its own reactive power output as well as to the voltages, operating states, and positions of adjacent network nodes. The coupled behavior indicates that correcting the voltage at one connection point can influence the voltage at another, which should be considered when selecting coordinated control settings for multiple PV units and compensation devices.

### 1.3) Effects of distributed PV on three-phase voltage unbalance

Distributed PV integration changes a low-voltage distribution network from a predominantly passive system into an active network with potentially bidirectional power flow. This transition affects the magnitude and direction of branch currents, while the intermittency of PV generation introduces further variation in the nodal voltage profile. Because individual PV units and customer loads may be connected to different phases, their unequal power injections can also increase three-phase voltage unbalance. Figure 3 provides a schematic representation of a low-voltage station area used to explain these effects. In the adopted model, the complex load at node $n$ is $P_n + jQ_n$, and the impedance of the line segment between nodes $n-1$ and $n$ is $R_n + jX_n$. A PV unit connected at a designated node injects active and reactive powers represented by $\Delta P_p$ and $\Delta Q_p$. These quantities provide the basis for assessing the resulting phase-specific voltage changes.

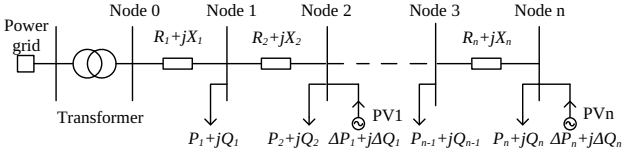


Figure 3: Schematic of distributed PV integration in a low-voltage station area

Figure 3 identifies the transformer, connected feeders, and distributed PV access points that influence the phase voltages in the station area. The simplified configuration allows the effect of one phase-connected PV unit to be discussed before the analysis is extended to multiple simultaneous PV injections. In practice, the locations of individual PV connections and the distribution of customer loads across phases both affect the resulting unbalance.

The analysis assumes that the original feeder supplies the loads connected at its nodes and that these loads remain independent of short-term PV generation variations. Consider first the connection of a PV unit to phase A, as represented by the feeder model in Figure 1. The voltage difference between the transformer's low-voltage terminal and the PV point of common coupling (PCC) can be described using the feeder's resistance and reactance. Before the additional PV injection is introduced, the corresponding approximate phase-A voltage drop is given by:

$$\Delta \dot{U}_A = \frac{r_n P_n + x_n Q_n}{U_n} + j\frac{x_n P_n - r_n Q_n}{U_n}, \qquad (6)$$

In Eq. (6), $r_n$ and $x_n$ represent the resistance and reactance between the transformer's low-voltage terminal and the common coupling point at node $n$, respectively. The parameter $U_n$ represents the node voltage magnitude. The voltage-drop expression is evaluated over the feeder section under the stated power-flow convention.

Eq. (6) relates the voltage drop to the active and reactive power transferred through the feeder and to the impedance between the transformer and the PCC. When distributed PV generation becomes available, the amount of power required from the upstream network decreases. With positive power flow defined toward the load, the resulting squared-voltage relationship between the supply terminal and the PV point of common coupling can be expressed as follows under the simplified branch model:

$$V_S^2 - V_P^2 = 2(RP + XQ) - (R^2 + X^2)\frac{P^2 + Q^2}{V_P^2}. \qquad (7)$$

The corresponding voltage-magnitude difference is obtained by dividing the difference of squared voltage magnitudes by the sum of those magnitudes:

$$\begin{aligned}\Delta V \equiv & V_S - V_P = \frac{V_S^2 - V_P^2}{V_S + V_P} \\ = & \frac{2(RP + XQ) - (R^2 + X^2)\frac{P^2+Q^2}{V_P^2}}{V_S + V_P},\end{aligned} \qquad (8)$$

The quantities $\Delta P_p$ and $\Delta Q_p$ represent the active and reactive power variations associated with PV injection, respectively. Distributed generation reduces the net demand supplied by the upstream network and changes the active and reactive power flowing through the feeder. The resulting voltage response depends on branch impedance, PV generation, local demand, and the direction of power transfer. In many forward-flow conditions, reduced line current decreases the voltage drop and raises the downstream node voltages. The resulting variations in phase voltage magnitudes and angles also influence three-phase voltage unbalance throughout the network.

ARCHIVES DES SCIENCES
A Multidisciplinary Journal

The electrical location of a PV connection influences the voltage change observed along the feeder. For the simplified single-PV case, the voltage deviation at an observation node is approximated by a piecewise relationship that depends on its distance from the station head relative to the PV connection distance. The resulting expression is written as follows:

$$\Delta \dot{U}_{Ai} = \begin{cases} \dfrac{l_i}{l_n}\Delta \dot{U}_n, & 0 \le l_i \le l_n, \\ \Delta \dot{U}_n, & l_n \le l_i \le l_N. \end{cases} \tag{9}$$

Here, $\Delta \dot{U}_{Ai}$ represents the voltage variation at node $i$ of phase A. The distance $l_i$ is measured from the station head to node $i$, $l_n$ denotes the distance from the station head to PV unit $n$, and $l_N$ represents the total branch line length.

When PV units connected to individual phases operate simultaneously, their phase-specific current injections produce different voltage variations at the observation nodes. In the simplified representation adopted here, the phase-A voltage variation at the PCC of node $i$ is related to the contributions of the connected units through the following summation. The corresponding phase-B and phase-C variations are considered analogously when evaluating the complete three-phase voltage profile:

$$\Delta V_i^A = -\sum_{n=1}^{N} Z_{i\leftrightarrow n} I_n^A = -\sum_{n=1}^{N} z\,|l_i - l_n|\, I_n^A. \tag{10}$$

The PV injection current may also be written in terms of the complex power $S_n^A = P_n^A + jQ_n^A$ and the local phase voltage $V_n^A$. Substituting this current relationship into Eq. (10) gives the equivalent representation below, where the asterisk denotes complex conjugation:

$$I_n^A = \frac{(S_n^A)^*}{(V_n^A)^*} \Rightarrow \Delta V_i^A = -\sum_{n=1}^{N} z \mid l_i - l_n \mid \frac{(S_n^A)^*}{(V_n^A)^*}. \tag{11}$$

Let $V_i^A$, $V_i^B$, and $V_i^C$ denote the three phase-to-neutral voltage phasors at the PCC of node $i$. Their positive-, negative-, and zero-sequence components are obtained using the standard symmetrical-component transformation shown below. These components provide an additional measure of the extent and character of three-phase voltage unbalance:

$$\begin{cases} V_i^+ = \dfrac{1}{3}(V_i^A + aV_i^B + a^2V_i^C), \\ V_i^- = \dfrac{1}{3}(V_i^A + a^2V_i^B + aV_i^C), \\ V_i^0 = \dfrac{1}{3}(V_i^A + V_i^B + V_i^C), \end{cases} \tag{12}$$

Here, $a = e^{j120^\circ}$ is the complex rotation operator representing a counterclockwise rotation of 120°. The quantities $\Delta \dot{U}_{Ai}$, $\Delta \dot{U}_{Bi}$, and $\Delta \dot{U}_{Ci}$ denote the voltage deviations in phases A, B, and C at node $i$, respectively. The sequence-component representation supports the analysis of phase balance under differing PV injection and compensation settings.

Following PV integration, the phase voltage magnitudes are used to calculate the average nodal voltage and the associated voltage unbalance rate (VUR). Eq. (13) defines the mean of the three phase voltage magnitudes, and Eq. (14) expresses the greatest absolute deviation from that mean as a percentage of the mean voltage. These indicators permit comparisons between nodal operating conditions before and after compensation. The VUR magnitude-deviation indicator is distinguished from the negative-to-positive sequence voltage ratio introduced later in Eq. (29); the two indices express related but not identical definitions of voltage unbalance.

$$V_{\mathrm{avg},i} = \frac{|V_i^A| + |V_i^B| + |V_i^C|}{3}, \tag{13}$$

$$\mathrm{VUR}_i(\%) = 100\% \times \frac{\max\left\{ \begin{array}{l} \left||V_i^A| - V_{\mathrm{avg},i}\right|, \\ \left||V_i^B| - V_{\mathrm{avg},i}\right|, \\ \left||V_i^C| - V_{\mathrm{avg},i}\right| \end{array} \right\}}{V_{\mathrm{avg},i}}. \tag{14}$$

After PV integration, voltage unbalance may be pronounced at or near a PV connection point, depending on phase allocation, feeder impedance, and the magnitude of local injections. Each node's voltage response depends jointly on nearby power variations and the impedance paths connecting that node to the PV sources. The location of maximum unbalance is therefore an outcome of network conditions rather than a universal characteristic of every PV-connected feeder. This observation highlights why compensation decisions should consider the full station-area voltage profile.

## III. Regulation Mechanism of Voltage Quality by Distribution Grid Reactive Power Compensators

Reactive power compensation is a principal means of addressing voltage deviation and phase-unbalance problems in low-voltage distribution networks. Conventional compensation resources, including static VAR generators (SVGs) and switched capacitor banks, are often installed near the distribution transformer, while distributed PV inverters can provide additional reactive power support within their available operating capability. Coordinating these resources can reduce the need to rely exclusively on transformer-side equipment and may improve voltage regulation at electrically distant nodes. The relationship between reactive power injection and nodal voltage variation provides a basis for identifying appropriate compensation locations, sizing requirements, and operating settings. In the proposed approach, PV reactive power, capacitor-bank switching, and SVG output are considered as complementary control resources. Their available outputs and operating restrictions are taken into account when seeking improved voltage regulation throughout the station area.

Capacitor banks are widely used reactive power compensation devices in distribution systems because of their comparatively straightforward construction and suitability for sustained operation. As capacitor banks are usually switched

ARCHIVES DES SCIENCES
A Multidisciplinary Journal

in discrete steps, they provide a finite number of compensation levels rather than continuously adjustable reactive power output. Their injection or absorption effect changes phase voltages through the impedance of the connected network. Phase-specific compensation can consequently contribute to reducing voltage unbalance, although the achievable improvement depends on how the banks are connected and operated. Appropriate coordination is required to avoid correcting one phase at the expense of unacceptable voltage changes in another.

For a particular phase, a change in reactive power injection alters the voltage at connected nodes through the associated network impedance. Under the simplified transformer-side approximation adopted here, the resulting complex voltage variation is expressed as follows:

$$\Delta\dot{U}_{CN} = \frac{X\Delta Q}{U_n} + j\frac{-R\Delta Q}{U_n} \tag{15}$$

In Eq. (15), $\Delta\dot{U}_{CN}$ represents the complex voltage variation associated with the capacitor bank on its connected phase. The variable $\Delta Q$ denotes the change in reactive power supplied by that bank; $R$ and $X$ are the effective transformer-side resistance and reactance, and $U_n$ represents the nominal voltage. This expression captures the voltage sensitivity to reactive compensation under the specified equivalent-network approximation.

When the output of reactive power compensation equipment is changed, the net phase voltage variations $\Delta\dot{U}_{Ai}$, $\Delta\dot{U}_{Bi}$, and $\Delta\dot{U}_{Ci}$ can be viewed as the combined effects of PV injections and compensation-device adjustments. The superposed responses help describe how simultaneous actions on different phases influence the resulting degree of voltage unbalance.

For illustration, consider changing only the capacitor-bank output connected to phase B while keeping the other control settings fixed. The corresponding change in the voltage-unbalance expression is subject to the permissible unbalance limit, as written below. The limit constrains the range of acceptable compensation adjustments, and any additional phase-specific bank changes must be evaluated for their combined effect on voltage quality.

$$\Delta\varepsilon_{U2i} = \frac{\left|a^2\dfrac{(X-jR)}{U_n}\Delta Q\right|}{\left|3U_i + a\dfrac{(X-jR)}{U_n}\Delta Q\right|} \le \Delta\varepsilon_{U2,\lim}, \tag{16}$$

Here, $\Delta\varepsilon_{U2,\lim}$ is the specified permissible change in voltage unbalance. This inequality constrains the compensation adjustment so that a calculated improvement in one voltage quality indicator does not exceed the allowed unbalance threshold.

## IV. Enhanced Algorithm for Particle Swarm Optimization

The particle swarm optimization (PSO) algorithm is a population-based search method in which candidate solutions, termed particles, update their positions using their own previously successful positions and information shared by the population. Unlike genetic algorithms, the basic PSO procedure does not require explicit crossover or mutation operators. Its implementation therefore involves relatively simple position and velocity updates, although its numerical performance remains sensitive to parameter selection and the formulation of constraints. In this work, PSO is applied to a station-area voltage regulation problem involving a mixture of discrete capacitor-bank switching decisions and continuously adjustable reactive power settings. An improved algorithm is introduced to encourage sufficient exploration of the feasible search space while supporting accurate adjustment of compensation variables.

The standard PSO method begins by initializing a population of particles at candidate positions within the allowable search space. Each particle is assigned a velocity and evaluated using an objective function that measures the quality of its proposed control settings. During successive iterations, each particle moves according to its current velocity, its best previously identified solution, and the best solution discovered by the population. The updated positions are then evaluated, and the individual and global best solutions are retained or replaced when superior candidate solutions are found. This iterative process continues until a stopping condition, such as a maximum iteration count or a convergence criterion, is met. The principal variables used to represent the candidate solutions and their movements are defined below:

Let $N$ denote the number of particles in the swarm and $D$ the number of optimization variables associated with each candidate solution. The $D$ variables may represent reactive power settings, capacitor switching states, or other station-area control decisions, as appropriate to the model. Every particle therefore occupies a point in a $D$-dimensional search space. The position vector of particle $i$ is defined as follows:

$$X_i = (x_{i1}, x_{i2}, \ldots, x_{iD}), \quad i = 1, 2, 3, \ldots, N. \tag{17}$$

The position vector describes the candidate values assigned to the control variables at a given iteration. A corresponding velocity vector determines the proposed change to those values during the next update. Position and velocity are therefore represented in the same number of dimensions, even when individual control variables have different permissible operating ranges or require special handling for discrete settings. For particle $i$, the velocity vector is written as:

$$V_i = (v_{i1}, v_{i2}, \ldots, v_{iD}), \quad i = 1, 2, 3, \ldots, N. \tag{18}$$

During the search, each particle retains the position at which it has achieved its best objective-function value so far. This is its individual or personal best position, commonly denoted by $P_{\text{best}}$ or $p_i$. For a $D$-dimensional particle, the stored individual best position can be represented as:

$$P_{\text{best}} = (p_{i1}, p_{i2}, \ldots, p_{iD}), \quad i = 1, 2, 3, \ldots, N. \tag{19}$$

ARCHIVES DES SCIENCES
A Multidisciplinary Journal

The swarm also records the position corresponding to the best objective-function value obtained among all particles during the optimization. This position is the global best, denoted by $g_{\text{best}}$. It acts as a shared reference that guides the search toward a promising region while individual best positions preserve information about the performance history of separate particles. The global best position is represented by the following vector:

$$g_{\text{best}} = (p_{g1}, p_{g2}, \ldots, p_{gD}), \quad i = 1, 2, 3, \ldots, N. \tag{20}$$

During an iteration, the particles use both personal and global best positions to update their velocities and then their positions. The inertia contribution retains part of the previous motion, while the two learning contributions encourage movement toward historically favorable solutions. In the notation adopted in this paper, the standard update relation is written as follows:

$$\begin{cases} v_{i(d+1)} = w v_{id} + c_1 r_1 (p_{id} - x_{id}) + c_2 r_2 (p_{gd} - x_{gd}), \\ x_{i(d+1)} = x_{id} + v_{id}, \end{cases} \tag{21}$$

where $w$ denotes the inertia weight, $c_1$ and $c_2$ are individual and population learning factors, and $r_1$ and $r_2$ are random numbers within the interval $[0, 1]$. The particle velocity is limited to the specified permitted range, and the position update establishes the candidate control settings for the next iteration. The personal best and global best positions provide the reference values used by the update terms.

In Eq. (21), the first term of the velocity update is the inertia contribution. It maintains some influence from the preceding particle velocity and therefore regulates the continuity of particle movement through the search space. The second term represents attraction toward the particle's own best previously observed position, while the third represents attraction toward the global best position. Their combined influence determines the balance between searching new regions and refining already promising candidate solutions. Because a large velocity can force control variables beyond their permissible limits, velocity bounds and feasible-position restrictions must be considered during optimization. Conversely, excessively small velocities may reduce exploration and slow convergence. The values of the inertia weight and learning factors are consequently important for obtaining satisfactory search behavior.

The conventional PSO procedure can be summarized by the following iterative steps, which are subsequently modified for the coordinated voltage regulation problem:

Step 1: Initialize the optimization parameters, the swarm size, the search-space dimensions, the admissible control-variable ranges, and the convergence settings.

Step 2: Generate initial particle positions and velocities within the permitted ranges so that the initial population represents candidate compensation settings.

Step 3: Evaluate the fitness of each initialized particle and establish its personal best position together with the best position discovered by the entire swarm.

Step 4: Update particle velocities and positions using Eq. (21), evaluate the resulting fitness values, and replace the personal best position whenever the new candidate provides a better objective-function value.

Step 5: Compare the updated personal best values to the current global best. When a particle produces a better feasible solution, update the global best position and retain the corresponding objective-function value.

Step 6: Terminate the process when the prescribed iteration or convergence condition is satisfied; otherwise, return to Step 4 and continue evaluating the updated population.

The station-area optimization problem is more complex than a purely continuous unconstrained search because the controllable variables include the switching states of capacitor-bank groups and the output levels of reactive power compensation devices. In addition, individual phase voltages, PV generation limits, and voltage-unbalance indicators must satisfy operational constraints. A feasible candidate therefore requires suitable values for several interdependent control quantities. These characteristics motivate adjustments to the basic PSO update mechanism, particularly the use of adaptive parameters and additional references to guide particle motion.

PSO performance depends substantially on the way its parameters are selected and updated. Excessive movement toward an early global best may reduce swarm diversity and cause premature convergence, while overly exploratory settings may prevent accurate refinement of promising solutions. To address these competing requirements, this study modifies the inertia weighting mechanism, adjusts the individual and population learning factors over the course of the optimization, and includes a reference to the best-performing particle within a specified neighborhood. Together, these changes seek to improve the ability to explore several candidate control configurations before selecting a set of compensation actions for the multiple voltage quality objectives.

1) Adaptive inertia weight $\omega$

The inertia weight determines how strongly a particle retains its previous velocity. A relatively large inertia weight can support exploration across a broad range of candidate solutions, whereas a smaller value generally encourages local refinement around promising regions. Consequently, maintaining an unchanging inertia weight throughout the optimization can limit flexibility when the character of the search changes between early and late iterations. The proposed approach varies this weight as a function of the particle fitness distribution to adjust the balance between global exploration and local search. In station-area reactive power optimization, such adaptation is intended to reduce premature convergence while preserving the accuracy required for phase-specific compensation settings. The following fitness-dependent expression is adopted for the inertia weight, subject to the definitions and limits specified by the implementation:

$$w = \begin{cases} w_{\min} + (w_{\max} - w_{\min}) e^{\frac{f^n_{\min} - f^n}{f^n_{\text{avg}} - f^n_{\min}}}, & f^n \le f^n_{\text{avg}}, \\ w_{\max}, & f^n > f^n_{\text{avg}}. \end{cases} \tag{22}$$

In Eq. (22), $w_{\min}$ and $w_{\max}$ represent the minimum and maximum inertia-weight parameters, $f^n_{\text{avg}}$ denotes the average fitness of all particles during iteration $n$, $f^n$ is the fitness of the particle being updated, and $f^n_{\min}$ is the best fitness at that iteration. The fitness-dependent exponential expression is intended to adjust the inertia contribution as the optimization proceeds. Numerical implementation must also handle equal fitness values and must enforce the intended operating bounds on the resulting weight.

2) Dynamic learning factors

The individual and social learning factors determine the strengths of attraction toward the personal and global reference positions. Their values influence how quickly particles converge and how widely the candidate settings are explored. Instead of fixing both factors for the entire calculation, the algorithm adjusts them according to the current iteration number relative to the allowed maximum. The update expressions for the two factors are stated as follows:

$$c_1(k) = c_{1,\min} + (c_{1,\max} - c_{1,\min}) \frac{k}{k_{\max}} \tag{23}$$

$$c_2(k) = c_{2,\min} + (c_{2,\max} - c_{2,\min}) \frac{k}{k_{\max}} \tag{24}$$

In Eqs. (23) and (24), $k$ is the current iteration number and $k_{\max}$ is the prescribed maximum number of iterations. The parameters $c_{1,\min}$ and $c_{1,\max}$ specify the lower and upper bounds of the individual learning factor, while $c_{2,\min}$ and $c_{2,\max}$ specify the corresponding bounds of the social learning factor. This linear adjustment changes the learning coefficients progressively as the search proceeds. The selection of parameter bounds remains important because it controls the relative contributions of a particle's personal search history and the population's shared information. The procedure provides a systematic way of varying the update behavior instead of requiring the same fixed learning coefficients at every stage.

3) Neighborhood reference variables

A standard global-best PSO population may lose diversity when many particles rapidly move toward the same reference position. To reduce this tendency, the proposed method introduces a further learning target based on the best-performing particle within a defined neighborhood. In addition to personal and global best positions, a particle therefore considers information obtained from nearby candidate solutions. This neighborhood reference provides another direction in which the particle can adjust its velocity and may help preserve alternative search paths. The resulting improved velocity update is written as $v_{i(d+1)} = wv_{id} + c_1 r_1 (p_{id} - x_{id}) + c_2 r_2 (p_{gd} - x_{gd}) + c_3 r_3 (p_{bd} - x_{id})$, where $p_{bd}$ is the best position in the selected neighborhood, $c_3$ is its learning factor, and $r_3$ is a random multiplier. Since the neighborhood contribution is intended to supplement rather than dominate the personal and global learning terms, the study imposes the condition $c_3 < c_1$ and $c_3 < c_2$. This additional reference can help particles examine potentially useful neighboring solutions while retaining the overall optimization objective. The improved procedural flow, including fitness evaluation and repeated parameter adjustment, is shown in Figure 4.

Figure 4 summarizes the iterative process of the improved PSO method. Following initialization, the inertia weight and learning factors are updated, the fitness of candidate control settings is evaluated, and particle positions are revised using the personal, global, and neighborhood references.

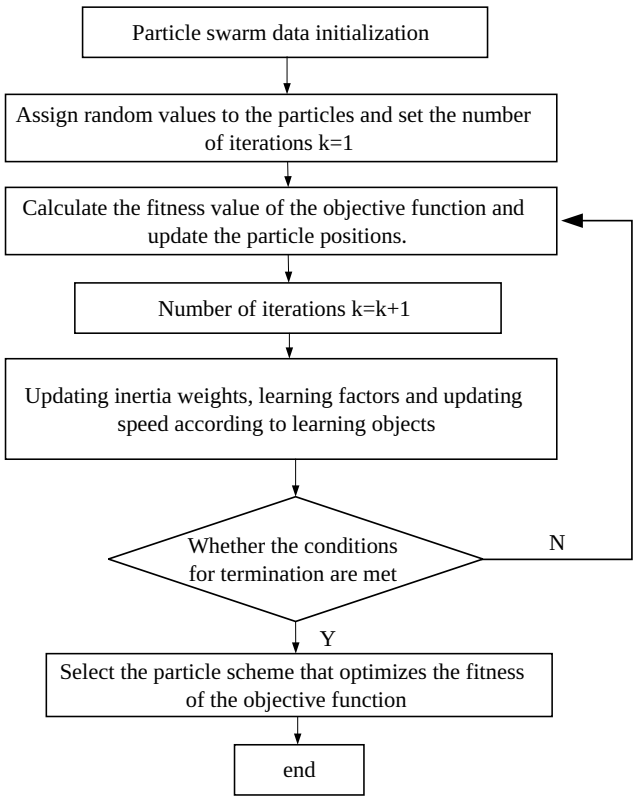


Figure 4: Flowchart of the improved particle swarm optimization procedure

The iterative search continues until a specified stopping condition has been satisfied. The diagram clarifies how the additional reference information is incorporated into the control-variable optimization process.

## V. Voltage Quality Correction through Coordinated Reactive Power Control in Station Areas

### A. Objective function

1) Expected voltage deviation index

The active power supplied by distributed PV systems changes with solar irradiance, while customer loads vary independently over time. These fluctuations can produce departures from the preferred nodal voltage levels, particularly on feeders

ARCHIVES DES SCIENCES
A Multidisciplinary Journal

with substantial PV penetration. As reactive power adjustments also affect voltages throughout the network, voltage deviation is included explicitly in the control objective. The proposed index considers the expected aggregate normalized deviation from the specified nodal reference values. By minimizing this index, the optimization seeks control settings that improve the station-area voltage profile under the modeled operating conditions. The first component of the objective function is defined as follows:

$$\min f_1 = E(\Delta U), \tag{25}$$

where the aggregate normalized voltage deviation is calculated from

$$\Delta U = \sum_{i=1}^{N_L} \left| \frac{U_i - U_i^{\text{ref}}}{U_{i,\max} - U_{i,\min}} \right|. \tag{26}$$

In Eqs. (25) and (26), $f_1$ is the expected aggregate voltage deviation, and $E(\cdot)$ denotes the expectation under the operating scenarios considered. The variable $N_L$ is the number of load nodes, $U_i$ is the voltage at node $i$, and $U_i^{\text{ref}}$ is its specified reference voltage. The terms $U_{i,\min}$ and $U_{i,\max}$ represent the lower and upper permissible voltages at that node, respectively. Normalizing each absolute voltage difference by the corresponding permitted voltage range allows deviations at different nodes to contribute on a comparable scale to the station-area control objective.

2) Expected three-phase voltage-unbalance index

Low-voltage distribution networks typically consist of a small number of three-phase high-power loads alongside a larger number of single-phase light loads. To ensure safe and reliable electricity supply, unbalanced loads are normally distributed across the three phases to balance power consumption. In an ideally balanced three-phase system, identical line and load parameters at all points of common coupling result in the presence of only the positive-sequence component. However, the variability of distributed PV generation and fluctuations in load demand disrupt the three-phase symmetry at certain nodes, leading to voltage unbalance. Consequently, addressing three-phase voltage imbalance is a critical concern for distribution network operation. To this end, the expected three-phase imbalance within the network is defined and employed as an optimization objective:

$$f_2 = E\left(U_{nb}\right), \tag{27}$$

where the sum of the node-level unbalance indices is given by

$$U_{nb} = \sum_{i=1}^{N_L} U_{inb}. \tag{28}$$

Here, $f_2$ denotes the expected station-area voltage-unbalance objective, $U_{nb}$ denotes the total unbalance index across the considered load nodes, and $U_{inb}$ represents the contribution from node $i$. Eq. (28) aggregates the node-level quantities, thereby allowing the optimization to consider phase quality throughout the feeder rather than only at one connection point. A commonly used negative-sequence definition of three-phase voltage unbalance is expressed below as a percentage of the positive-sequence component:

$$\varepsilon_{U2} = \frac{U_2}{U_1} \times 100\% \tag{29}$$

Here, $\varepsilon_{U2}$ denotes the voltage-unbalance factor, calculated as the ratio of the root-mean-square negative-sequence voltage magnitude $U_2$ to the positive-sequence voltage magnitude $U_1$, expressed as a percentage.

The sequence components at PCC node $i$ are obtained from the three phase voltage phasors and their PV- and compensation-induced variations through the following transformation:

$$\begin{bmatrix} \dot{U}_{A_1} \\ \dot{U}_{A_2} \\ \dot{U}_{A_0} \end{bmatrix} = \frac{1}{3} \begin{bmatrix} 1 & a & a^2 \\ 1 & a^2 & a \\ 1 & 1 & 1 \end{bmatrix} \begin{bmatrix} \dot{U}_A + \Delta\dot{U}_{Ai} \\ \dot{U}_B + \Delta\dot{U}_{Bi} \\ \dot{U}_C + \Delta\dot{U}_{Ci} \end{bmatrix}, \tag{30}$$

Here, $a = e^{j120^\circ}$ denotes the symmetrical-component rotation operator. The phase voltage variations $\Delta\dot{U}_{Ai}$, $\Delta\dot{U}_{Bi}$, and $\Delta\dot{U}_{Ci}$ describe the effects of PV generation and compensation adjustments at node $i$. The transformed voltage quantities are used to evaluate the resulting sequence-component unbalance.

The expected voltage deviation from Eq. (25) and expected voltage unbalance from Eq. (27) are combined in a weighted multi-objective function. The formulation treats the two performance indices as complementary criteria whose relative importance is controlled by the chosen weights:

$$F = \min\left(\lambda_1 f_1 + \lambda_2 f_2\right), \tag{31}$$

where $\lambda_1$ and $\lambda_2$ are the nonnegative weighting coefficients for voltage deviation and voltage unbalance, respectively. These coefficients allow the control objectives to be balanced according to station-area operating priorities. Their admissible values satisfy the following normalization conditions:

$$\begin{cases} \lambda_1 + \lambda_2 = 1, \\ 0 \le \lambda_1 \le 1, \\ 0 \le \lambda_2 \le 1. \end{cases} \tag{32}$$

The weighting coefficients can be selected using an analytic hierarchy process (AHP) in which relative priorities are assigned to the considered criteria. Their actual numerical values must be specified for any reproducible optimization run. The normalization in Eq. (32) ensures that both terms are considered within one combined objective function, rather than being treated as unrelated optimization tasks.

### *B. Operating constraints*

Reactive power optimization in the distribution station area is subject to both equality and inequality constraints. The

equality conditions comprise the active and reactive power-flow balances at the nodes, ensuring that candidate operating points satisfy the assumed electrical network model. The inequality constraints represent equipment output limits, permissible node voltages, and bounds on reactive compensation resources and transformer control settings. These restrictions are necessary because a numerical reduction in the objective function is not acceptable if it would require an inverter, a capacitor bank, or another device to operate outside its permitted range. Feasibility is therefore considered alongside the improvement of voltage deviation and phase unbalance.

1) Equality constraints

The nodal power-flow equations constitute the equality constraints for reactive power optimization. They represent active and reactive power balance between generation, load demand, and electrical transfers at each node. The corresponding expressions, based on the specified network admittance relationships, are written as follows:

$$\begin{aligned} P_i^{gen} - P_i^{load} &= \sum_{j\in\Omega_i} V_i V_j \left(G_{ij}\cos\theta_{ij} + B_{ij}\sin\theta_{ij}\right), \\ Q_i^{gen} - Q_i^{load} &= \sum_{j\in\Omega_i} V_i V_j \left(G_{ij}\sin\theta_{ij} - B_{ij}\cos\theta_{ij}\right), \end{aligned} \tag{33}$$

where $P_i^{gen}$ and $Q_i^{gen}$ represent active and reactive generation at node $i$, while $P_i^{load}$ and $Q_i^{load}$ are the corresponding loads. The terms $V_i$ and $V_j$ denote voltage magnitudes, $G_{ij}$ and $B_{ij}$ are the conductance and susceptance terms in the network model, $\theta_{ij}$ is the voltage phase-angle difference, and $\Omega_i$ identifies the nodes included in the relevant summation. The power-flow conditions must be satisfied by the candidate compensation settings before the corresponding voltage quality indices can be meaningfully evaluated.

2) Inequality constraints

Operational state variables and reactive power resources are restricted to their prescribed feasible ranges through the following inequality constraints:

$$\begin{cases} U_{i,\min} \le U_i \le U_{i,\max}, \\ Q_{i,C,\min} \le Q_{i,C} \le Q_{i,C,\max}, \\ Q_{i,SVG,\min} \le Q_{i,SVG} \le Q_{i,SVG,\max}, \end{cases} \tag{34}$$

In Eq. (34), $U_i$ is the voltage at phase node $i$, and $U_{i,\min}$ and $U_{i,\max}$ are its lower and upper permissible voltage limits. The variables $Q_{i,C}$ and $Q_{i,SVG}$ denote reactive power output from the capacitor bank and static VAR generator, respectively. The corresponding minimum and maximum subscripts identify the permissible operating limits of each compensation device.

Each distributed generation unit must also operate within its specified active and reactive power output limits, as expressed by the following inequalities:

$$\begin{cases} P_{Gm,\min} \le P_{Gm} \le P_{Gm,\max}, \\ Q_{Gm,\min} \le Q_{Gm} \le Q_{Gm,\max}, \end{cases} \tag{35}$$

where $P_{Gm}$ and $Q_{Gm}$ are the active and reactive power supplied to the system by the mth unit.

If an adjustable transformer ratio is included as a control variable, it must remain within its permitted tap-ratio bounds:

$$t_{ij,\min} \le t_{ij} \le t_{ij,\max}. \tag{36}$$

Reliable power supply requires all nodal voltage magnitudes to remain within the admissible range. In addition to the node-specific limits in Eq. (34), a common overall voltage bound may be imposed on the network, as stated below:

$$U_{\min} \le U_i \le U_{\max}. \tag{37}$$

After determining the objective function, network operating constraints, and feasible control variables, the coordinated optimization procedure follows the algorithmic structure illustrated in Figure 5.

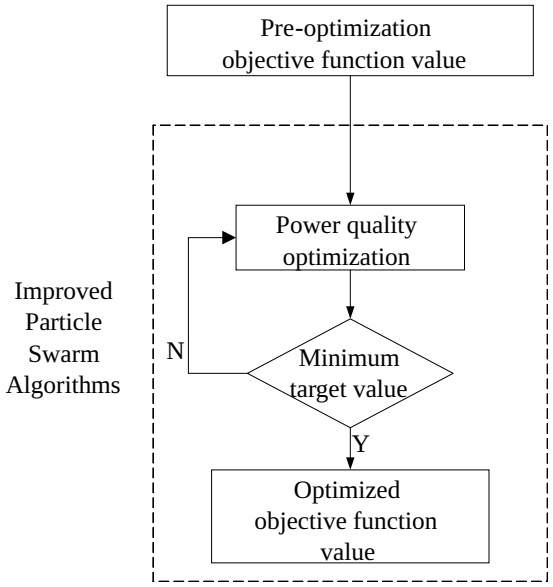


Figure 5: Coordinated station-area voltage quality regulation using improved particle swarm optimization

Figure 5 illustrates the coordinated voltage quality regulation procedure using PV reactive power support and conventional compensation equipment. The improved PSO routine evaluates candidate compensation settings against the weighted objective function and rejects or constrains settings that violate the modeled equipment and voltage limits. The sequence of calculations therefore links the network's voltage quality indicators to operationally feasible control actions, rather than optimizing the performance indices in isolation.

## VI. Results and Analysis

The proposed coordinated voltage quality regulation method is assessed using simulations of a 380-V low-voltage distribution network in Jiangsu Province, China, under a representative sunny summer-day operating condition. The modeled station area contains an SCB10-160 transformer rated at 160

ARCHIVES DES SCIENCES
A Multidisciplinary Journal

kVA, one capacitor bank, four distributed PV systems, and 29 users. The individual single-phase customer loads are assigned to the network nodes to form a three-phase system with a grounded neutral conductor. This arrangement permits the effects of unequal phase loading and phase-specific PV power injections to be examined. The station-area configuration is shown in Figure 6. The transformer's high-voltage side is connected to an upstream network represented by an infinite bus, for which the source voltage is assumed constant throughout the simulated period.

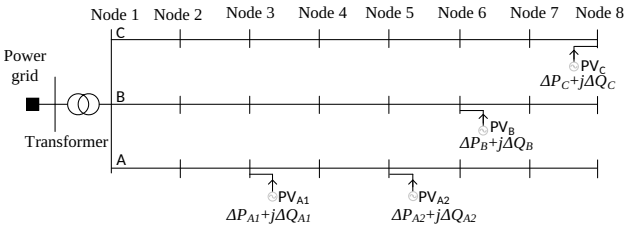


Figure 6: Configuration of the low-voltage distribution station-area simulation model

Figure 6 provides a schematic of the station-area simulation configuration. The modeled elements include the transformer connection, low-voltage feeder structure, PV installations, and reactive power control resources relevant to the voltage quality assessment. The configuration supports comparisons between independent reactive power regulation and the coordinated settings obtained through the improved PSO algorithm.

The simulated feeder voltage profiles are compared in Figures 7 and 8. During the daylight evaluation interval from 06:00 to 18:00, the coordinated control strategy is reported to reduce the main-feeder voltage deviation by an average of 30.72% relative to independent reactive power regulation. The coordinated approach draws on existing station-area compensation resources together with the reactive power capability available from distributed PV systems. Within the simulated configuration, this coordination does not require installing an additional dedicated compensation device. Its performance nevertheless depends on the available inverter reactive power capability, which is constrained by equipment ratings and the prevailing active power output. The relationship between active power generation and available reactive power is governed by the inverter's apparent-power limit; consequently, an increased PV active power output does not automatically imply an increased reactive power margin. During periods with little or no PV generation, capacitor-bank switching can remain useful for correcting voltage deviations, subject to its discrete switching capability and the assumptions concerning inverter operation. The combined strategy is therefore intended to use each available resource according to its operational strengths. The simulation results indicate improved voltage regulation at both the beginning and the end of the main feeder, thereby supporting the effectiveness of the coordinated control method under the tested conditions.

Figure 7 shows the variation of voltage at the beginning of the main feeder during the evaluated operating period. The comparison provides a feeder-head perspective on the effect of the proposed control strategy and complements the end-of-feeder analysis in Figure 8. Voltage changes at the feeder head reflect the combined impact of station-area loading, PV generation, and reactive power control settings.

Figure 8 presents the voltage variation at the end of the main feeder before and after application of the improved PSO-based regulation approach. The end-of-feeder location is important because voltage deviations can be amplified by the impedance and cumulative power flow along a radial distribution line. Considering both Figures 7 and 8 provides a more complete comparison of the voltage regulation effect than examining only one monitoring point.

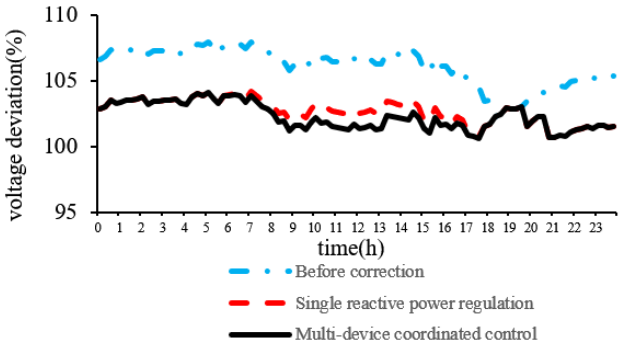


Figure 7: Voltage variation at the head of the main feeder

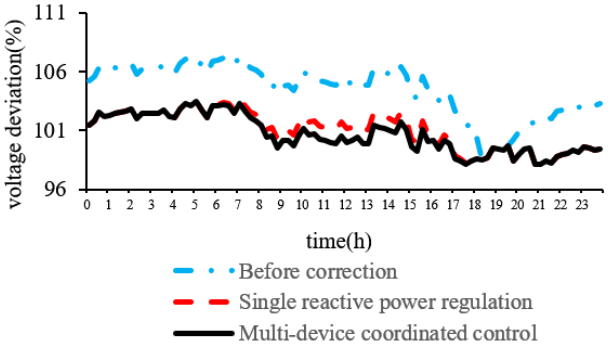


Figure 8: Voltage variation at the end of the main feeder

The node-level three-phase voltage-unbalance results before and after optimization are compared in Figures 9 and 10. The simulations indicate a reduction in the degree of unbalance at several representative nodes. At node 6, the reported unbalance decreases from a value close to 2% before optimization to below 1.5% afterward. At node 7, the initial unbalance of approximately 3% falls below 2% following the coordinated control adjustment. These reported changes indicate that the proposed algorithm can improve phase balance while regulating the main-feeder voltage profile. The extent of improvement varies between nodes because their electrical positions, connected loads, and PV injection conditions differ.

The comparison therefore supports assessing voltage regulation and phase unbalance together rather than relying on one network-wide indicator alone.

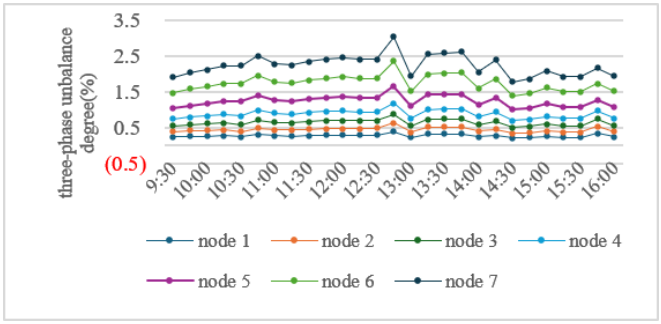


Figure 9: Three-phase voltage unbalance at network nodes before optimization

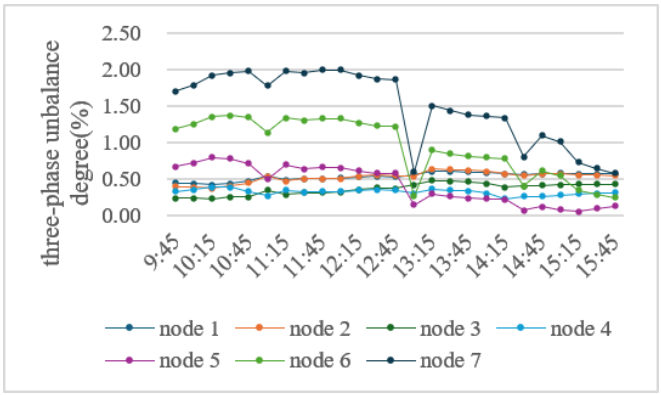


Figure 10: Three-phase voltage unbalance at network nodes after optimization

The reported results suggest that the proposed coordinated regulation method mitigates three-phase voltage unbalance associated with distributed PV integration while maintaining the principal voltage regulation objectives of the station area.

Figure 9 provides the node-by-node three-phase unbalance results before optimization. These initial values establish a reference for assessing the changes obtained from the coordinated control procedure. Differences between nodes reflect the spatial distribution of load conditions, PV injections, and the corresponding network voltage responses.

Figure 10 shows the corresponding three-phase unbalance results after application of the improved PSO regulation strategy. Comparison with Figure 9 indicates that the unbalance levels at the reported nodes are reduced, consistent with the quantitative examples discussed above. The results suggest an improvement in phase-voltage quality under the simulated operating condition, although performance under other PV generation and loading scenarios would require additional validation.

## VII. Conclusion

This study proposed an improved particle swarm optimization-based voltage quality regulation method for a low-voltage distribution station area with integrated distributed PV generation. By examining the effects of single and multiple PV connections and coordinating reactive power compensation resources, the proposed approach addresses voltage deviation and three-phase unbalance within a common optimization framework. Adaptive inertia weighting, dynamically adjusted learning factors, and a neighborhood-best reference were introduced to support the PSO search process. Simulation of a representative 380-V station area in Jiangsu Province indicated that the coordinated strategy improved voltage regulation compared with independent reactive power compensation. The reported daytime main-feeder voltage deviation decreased by an average of 30.72%, while the three-phase voltage unbalance at representative nodes was also reduced. These findings illustrate the potential value of coordinating existing compensation devices with the reactive power capabilities of distributed PV inverters, subject to the operating limits of the equipment. Future evaluation across additional PV penetration levels, seasonal load conditions, and network configurations would help establish the method's wider applicability and practical robustness.

The principal abbreviations and notation used in the proposed voltage quality regulation model are summarized in Table 1. The table is intended to support consistent interpretation of the power-flow equations, PSO control parameters, and voltage quality indicators throughout the manuscript.

## List of Abbreviations

Table 1: Abbreviations and principal notation used in the manuscript

| Abbreviation | Definition |
|---|---|
| PV | Photovoltaic |
| PSO | Particle Swarm Optimization |
| IPSO | Improved Particle Swarm Optimization |
| SVG | Static Var Generator |
| LV | Low Voltage |
| DG | Distributed Generation |
| GPQI | Global Power Quality Index |
| AHP | Analytic Hierarchy Process |
| MSOGI | Multi-Second-Order Generalized Integrator |
| R | Resistance |
| X | Reactance |
| P | Active Power |
| Q | Reactive Power |
| U | Voltage Magnitude |
| $\omega$ | Inertia Weight (PSO parameter) |
| $P_{\text{best}}$ | Particle's Individual Best Position |
| $g_{best}$ | Global Best Position |
| $p_{bd}$ | Best Position Among Neighboring Particles |
| T | Iteration Number |
| $T_{max}$ | Maximum Number of Iterations |
| $f_n$ | Fitness Value of a Particle |
| $U_{i,max}/U_{i,min}$ | Upper and Lower Voltage Limits at Node $i$ |
| $Q_{i,C}/Q_{i,SVG}$ | Reactive Power of Capacitor and SVG at Node $i$ |
| $\varepsilon_{U2}$ | Three-Phase Voltage Unbalance Degree |
| $U_1/U_2$ | Positive and Negative Sequence Voltage Components |
| $\lambda_1, \lambda_2$ | Weighting Coefficients in Multi-Objective Function |
| $R_n/X_n$ | Resistance and Reactance Between Nodes |
| $N_L$ | Number of Load Nodes |
| $P_{DG,i}/Q_{C,i}$ | Active and Reactive Power of Distributed PV and Compensation Equipment |
| $t_{ij}$ | Transformer Ratio |
| SCB | Dry-Type Transformer (e.g., SCB10-160) |

## Authors' Contributions

Jian Liu and Hui Fu contributed to the study design, development of the proposed framework, performance analysis, validation of the simulation results, and preparation of the manuscript. Mingming Shi and Xian Zheng contributed to the collection and organization of information required for the framework, provision of software-related support, critical review of the manuscript, and administration of the research process. All authors are responsible for reviewing and approving the final manuscript before submission.

## Conflict of Interest

The authors declare that they have no conflicts of interest.

## Data Availability

The data supporting the findings of this study are available from the corresponding author upon reasonable request. Availability may be subject to the applicable organizational data-sharing requirements.

## Funding

This work was supported in part by the State Grid Jiangsu Electric Power Co., Ltd. under Grant J2022041.

## References

[1] Tang, G. L. (2024). Research on the impact and control technology of distributed photovoltaic grid-connected power generation on the power grid. *Electric Power System Equipment*, (4), 59–61.

[2] Chen, Q., Bai, J., Chen, X. Y., Wang, Y., Wang, H. Y., Zhou, Y. B., Wang, F. Y., & Dong, N. (2024). Review of the impact of distributed PV grid integration on the power grid. *Science Technology and Engineering*, *24*(27), 11491–11504.

[3] Lin, Y., Gu, T., Qiu, X. D., & Li, X. D. (2023). Study on the influence of distributed photovoltaics on power quality in household distribution networks. *Chinese Journal of Electron Devices*, *46*(2), 561–566.

[4] Yuan, J. D., Chen, S. S., Li, D. Z., Zhou, Y., & Chen, K. (2021). Study on the evolution law of typical characteristics of distributed photovoltaic under the influence of various factors. *Distribution & Utilization*, *38*(3), 72–77.

[5] Qu, G. Q. (2021). Location and capacity research of distributed photovoltaic integrated in distribution network feeder considering multiple influence factors. *Electrical Measurement & Instrumentation*, *58*(5), 130–136, 158.

[6] Yu, H. N., Huang, L., Zhang, S. D., Chen, H. Q., Tang, C., & Huang, Y. H. (2020). Effects of distributed photovoltaic generation and electric vehicle integrating into distribution network on line loss and voltage drift. *Smart Power*, *48*(1), 28–34.

[7] Fu, Z. X., Wang, J. J., Zhu, J. P., & Yuan, Y. (2020). Impact of distributed photovoltaic access on forecast results of sag regions in distribution networks. *Chinese Journal of Power Sources*, *44*(10), 1518–1521, 1548.

[8] Bedawy, A., Yorino, N., Mahmoud, K., & Lehtonen, M. (2021). An effective coordination strategy for voltage regulation in distribution system containing high intermittent photovoltaic penetrations. *IEEE Access*, *9*, 117404–117414. https://doi.org/10.1109/ACCESS.2021.3106838.

[9] Cheng, L., Li, X., Xiang, X. Y., Qi, Y. Q., & Liu, L. Y. (2021). Research on the influence of distributed photovoltaic access on distribution network voltage based on power flow calculation. *Bulletin of Science and Technology*, *37*(5), 31–36, 112.

[10] Liu, F., Liu, J., Liu, Q., & Han, Y. (2024). Analysis of power quality and additional loss in distribution network with distributed generation. *Electric Power Systems Research*, *234*, Article 110834. https://doi.org/10.1016/j.epsr.2024.110834.

[11] Ravi, T., & Sathish Kumar, K. (2022). Analysis, monitoring, and mitigation of power quality disturbances in a distributed generation system. *Frontiers in Energy Research*, *10*, Article 989474. https://doi.org/10.3389/fenrg.2022.989474.

[12] Bandopadhyay, S., Bandyopadhyay, A., Mondal, A., & Sadhu, P. K. (2024). Harmonics reduction and power quality improvement in distributed power flow controller by SVPWM and MGWO technique. *Microsystem Technologies*, *30*, 1231–1238.

[13] Adchaya, J. S., & Kumar, C. A. (2024). Adaptive hybrid NFS-MSOGIQ control technique for improving power quality in solar PV distributed generation system. *Electric Power Components and Systems*, *52*(11), 2109–2124. https://doi.org/10.1080/15325008.2024.2317360.

[14] Boulanouar, S. A., Kaddouri, A. M., Kouzou, A., Benaissa, A., Teta, A., Hafaifa, A., Kennel, R., & Abdelrahem, M. (2023). Multifunctional control technique for grid-tied hybrid distributed generation system taking into account power quality issues. *Energies*, *16*(18), Article 6565. https://doi.org/10.3390/en16186565.

[15] Gu, Z. L., Zhao, Z. Y., Dong, Z. Y., & Wang, J. (2024). The research on power quality management technology of station area based on distributed photovoltaic scale access. *Journal of Physics: Conference Series*, *2703*(1), Article 012061. https://doi.org/10.1088/1742-6596/2703/1/012061.

[16] Afandi, I., Agalgaonkar, A. P., & Perera, S. (2022). Integrated Volt/Var control method for voltage regulation and voltage unbalance reduction in active distribution networks. *Energies*, *15*(6), Article 2225. https://doi.org/10.3390/en15062225.

[17] Mendoza, L., Saavedra-Montes, A., & Ramos-Paja, C. (2023). Formulation of a power quality index of a radial distribution network with distributed generation. In *2023 11th International Conference on Power Electronics and ECCE Asia (ICPE 2023–ECCE Asia)* (pp. 580–586). IEEE.

[18] Yu, D. W., Zhang, Y., Wang, Q. Y., & Su, Y. Z. (2023). Research and governance of power quality of the distribution network based on large-scale distributed PV access. *Journal of Physics: Conference Series*, *2477*(1), Article 012014. https://doi.org/10.1088/1742-6596/2477/1/012014.

[19] Chen, Y., Tang, Z., Weng, X., He, M., Zhang, G., Yuan, D., & Jin, T. (2024). A novel approach for evaluating power quality in distributed power distribution networks using AHP and S-transform. *Energies*, *17*(2), Article 411. https://doi.org/10.3390/en17020411.

[20] Qu, Y., Shi, M., Sun, S., Li, B., Fei, J., & Yang, X. (2023). Three-phase unbalance control method based on coordinated control of adjustable resources in distribution network. In *2023 5th Asia Energy and Electrical Engineering Symposium (AEEES)* (pp. 784–789). IEEE. https://doi.org/10.1109/AEEES56888.2023.10114130.

[21] Sun, S., Shi, M., Qu, Y., Li, B., Fei, J., & Yang, X. (2023). Coordination control strategy of distribution grid voltage based on adjustable resources in substation area. In *2023 5th Asia Energy and Electrical Engineering Symposium (AEEES)* (pp. 87–93). IEEE. https://doi.org/10.1109/AEEES56888.2023.10114098.

[22] Zhang, S., Yan, J., Xie, P., Zhai, P., & Tao, Y. (2025). Power system loss reduction strategy considering security constraints based on improved particle swarm algorithm and coordinated dispatch of source–grid–load–storage. *Processes*, *13*(3), Article 831. https://doi.org/10.3390/pr13030831.

[23] Zhou, F., Xiao, Y., Yao, T., Xie, F., & Bian, J. (2025). Suitability of photovoltaic power station sites based on particle swarm optimization model of fuzzy hierarchical analysis: Taking Qujing City of Yunnan Province as example. *Energies*, *18*(5), Article 1124. https://doi.org/10.3390/en18051124.

[24] Yang, X., Zhang, L., & Han, X. (2025). Electric vehicle charging load forecasting method based on improved long short-term memory model with particle swarm optimization. *World Electric Vehicle Journal*, *16*(3), Article 150. https://doi.org/10.3390/wevj16030150.